This is the peer-reviewed, final accepted version for American Mineralogist, published by the Mineralogical Society of America.
The published version is subject to change. Cite as Authors (Year) Title. American Mineralogist, in press.
DOI: https://doi.org/10.2138/am-2021-7575. http://www.minsocam.org/

Revision 2 Word Count: 7509

Phase transitions among $CaCO_3$ crystal structures under hydrous and anhydrous conditions: Implications for the structural transformation of $CaCO_3$ during subduction processes

Xueyin Yuan[1*], Robert A. Mayanovic[2] and Guoliang Zhang[3]

[1] MNR Key Laboratory of Metallogeny and Mineral Assessment, Institute of Mineral Resources, Chinese Academy of Geological Sciences, Beijing 100037, China

[2] Department of Physics, Astronomy and Material Science, Missouri State University, Springfield, MO 65897, USA

[3] Key Laboratory of Marine Geology and Environment & Center of Deep Sea Research, Institute of Oceanology, Chinese Academy of Sciences, Qingdao 266071, China

Abstract: The transport of calcium carbonate ($CaCO_3$) into the Earth's interior through subduction is one of the key processes in the global cycling of carbon. For developing a better understanding of the $CaCO_3$ structural chemistry during subduction processes, the phase transitions among $CaCO_3$-I (calcite), $CaCO_3$-II, III/IIIb and aragonite under pressure-temperature (*P*-*T*) conditions up to 2.5 GPa and 600°C, in hydrous and anhydrous environments, were investigated using a hydrothermal diamond anvil cell. One displacive and two reconstructive processes during the phase transitions among $CaCO_3$ polymorphs were confirmed from the results as obtained from in-situ observations and Raman spectroscopic measurements, meanwhile the effect of Ca-substitutional metal cations (e.g., Mg^{2+}) in $CaCO_3$ and the presence of an aqueous fluid on the phase transition processes have been determined. Specifically, the $CaCO_3$-I ↔ II phase transition is a displacive process, occurring instantly at pressures varying from 1.6 GPa at room temperature to 1.5 GPa at 500°C with the phase

* Corresponding author, Email: xueyinyuan@live.com

Always consult and cite the final, published document. See http:/www.minsocam.org or GeoscienceWorld

This is the peer-reviewed, final accepted version for American Mineralogist, published by the Mineralogical Society of America.
The published version is subject to change. Cite as Authors (Year) Title. American Mineralogist, in press.
DOI: https://doi.org/10.2138/am-2021-7575. http://www.minsocam.org/

equilibrium boundary having a minimum *P-T* point at approximately 1.4 GPa at 300°C, and is completely reversible upon cooling and decompression. The $CaCO_3$-II → III phase transition is a reconstructive process, observed at *P-T* conditions increasing from 2.0 GPa at room temperature to 2.5 GPa at 150°C, and is accomplished by solid recrystallization starting from $CaCO_3$-II, transitioning through an intermediate $CaCO_3$-IIIb, and ending at the $CaCO_3$-III crystal structure. The phase transition between $CaCO_3$-I or II and aragonite, which is also a reconstructive process, was found to occur by progressive solid recrystallization under high *P-T* hydrous and anhydrous conditions, or alternatively, via dissolution-precipitation under low *P-T* hydrous conditions, depending upon the presence of aqueous fluids and the heating rate of the system. The substitution for Ca^{2+} by other metal cations (e.g., Mg^{2+}, Mn^{2+}, Fe^{2+}) in $CaCO_3$ results in significant increase in the pressures for the displacive and solid recrystallization reconstructive phase transitions, but has no detectable influence on the $CaCO_3$-I/II ↔ aragonite transformation via a dissolution-precipitation process under hydrous conditions. Our results show that the presence of Ca-substitutional metal cations in $CaCO_3$ is a key factor controlling the stability of the $CaCO_3$ crystal structures under high *P-T* conditions, and suggest that aragonite should be the predominant crystal structure in the upper mantle in subduction zones where the heating rate is very low and slab dehydration is prevalent.

Key words: Calcite, $CaCO_3$-II, $CaCO_3$-III/IIIb, aragonite, phase transition, subduction

Always consult and cite the final, published document. See http:/www.minsocam.org or GeoscienceWorld

This is the peer-reviewed, final accepted version for American Mineralogist, published by the Mineralogical Society of America.
The published version is subject to change. Cite as Authors (Year) Title. American Mineralogist, in press.
DOI: https://doi.org/10.2138/am-2021-7575. http://www.minsocam.org/

Introduction

Calcium carbonate ($CaCO_3$) is one of the most important carbon-bearing substances on our planet. It determines the residence time of carbon in the deep ocean and sedimentary rocks, and acts as the major carrier for carbon during the transfer of subducted oceanic crust into the deep earth (Wallmann and Aloisi, 2012). Despite major portions of subducted carbonates becoming assimilated by basaltic magmas (Carter and Dasgupta, 2015; Seto et al., 2008; Spandler et al., 2012), inclusions from diamonds demonstrate that part of the carbonates may survive and be transported into the deep mantle (Brenker et al., 2007; Gao et al., 2017; Martirosyan et al., 2019). Studying the phase transitions of $CaCO_3$ and the structural chemistry of high *P-T* $CaCO_3$ phases are of fundamental importance for predicting the occurrence states of carbon in the deep earth (Dasgupta and Hirschmann, 2010; Litasov and Ohtani, 2009), and their contributions to the anomalies in the physicochemical properties (e.g., buoyancy) of subducted slabs (Li et al., 2015; Litasov et al., 2017). To date, at least ten crystal structures of $CaCO_3$ have been known to exist, among which $CaCO_3$-I (generally known as calcite) is consensually recognized as the stable phase on the earth's surface and in the shallow crust, and $CaCO_3$-VII as the stable phase at *P-T* conditions corresponding to the bottom of the earth's upper mantle and post aragonite in the earth's lower mantle, respectively (Bagdassarov and Slutskii, 2010; Bayarjargal et al., 2018; Bridgman, 1938; Davis, 1964; Irving and Wyllie, 1973; Li et al., 2018; Liu and Mernagh, 1990; Merlini et al., 2012; Mirwald, 1976; Oganov et al., 2006; Ono et al., 2005; Suito et al., 2001).

However, the phase relations among $CaCO_3$-I, II, III/IIIb and aragonite are still controversial: According to the results from thermodynamic simulations, the $CaCO_3$-I ↔ aragonite equilibrium

Always consult and cite the final, published document. See http:/www.minsocam.org or GeoscienceWorld

This is the peer-reviewed, final accepted version for American Mineralogist, published by the Mineralogical Society of America.
The published version is subject to change. Cite as Authors (Year) Title. American Mineralogist, in press.
DOI: https://doi.org/10.2138/am-2021-7575. http://www.minsocam.org/

61 phase boundary extends from ~0.4 GPa at room temperature to ~1.0 GPa at 500°C at a slightly
62 increasing positive $\partial P/\partial T$ slope (Johannes and Puhan, 1971; Redfern et al., 1989). However, during
63 high pressure experiments $CaCO_3$-I was generally preserved under pressures above the $CaCO_3$-I ↔
64 aragonite phase boundary, then transformed into a $CaCO_3$-II structure at pressures varying from
65 around 1.6 GPa under room temperature to 2.1 GPa at 650°C through a minimum point at about 1.3
66 GPa and 300°C (Bridgman, 1938; Kondo et al., 1972; Pippinger et al., 2015). With increase in
67 pressure $CaCO_3$-II transformed to $CaCO_3$-III/IIIb at 2.0 GPa and further to a $CaCO_3$-VI structure at
68 15 GPa and ambient temperature conditions (Bridgman, 1938; Liu and Mernagh, 1990; Merlini et al.,
69 2012; Pippinger et al., 2015; Yuan et al., 2018). Since their *P-T* stability fields lie within those of
70 aragonite and $CaCO_3$-II and III/IIIb have lower densities than aragonite under the same *P-T*
71 conditions, these structures are generally considered to be metastable phases (Bayarjargal et al., 2018;
72 Merlini et al., 2012; Merrill and Bassett, 1975). The basis for their occurrence in the *P-T* stability
73 space of aragonite has not yet been properly established.

74 The *P-T* conditions for the phase transitions among $CaCO_3$ polymorphs are also affected by the
75 incorporation of metal cations into $CaCO_3$. For instance, with progressive substitution for Ca^{2+} by
76 metal cations having smaller radii (e.g., Mg^{2+}, Mn^{2+}, Fe^{2+}) in calcite, the *P-T* stability field of the
77 $CaCO_3$-I structure is increased and the solid solution may transform directly into $CaCO_3$-VI without
78 going through the $CaCO_3$-II and III structures (Liu et al., 2016; Shi et al., 2012). The $CaCO_3$-I ↔
79 aragonite transformation rate has been shown to be kinetically hindered, with particularly slow rates
80 at temperatures below 200°C, and to be dependent, in addition to temperature, upon crystallite size
81 and presences of volatiles (Davis and Adams, 1965; Hacker et al., 1992; Liu and Yund, 1993;

Perdikouri et al., 2008). These developments notwithstanding, the phase transition mechanisms among $CaCO_3$-I, II, III/IIIb and aragonite and, in particular, the impact of aqueous fluids and Ca-substitutional metal cations on the transformation processes, need to be fully elucidated. In this paper, we present the results from in-situ microscopic observations and Raman spectroscopic measurements of the phase transitions among $CaCO_3$-I, II, III/IIIb and aragonite under *P-T* conditions up to 2.5 GPa and 600°C, and in hydrous and anhydrous environments. By combining our findings with those from previous studies, we establish a comprehensive understanding of the phase relations among the $CaCO_3$ polymorphs, which can be applied in predicting the structural transformations of $CaCO_3$ during subduction processes.

Experimental methods

The starting materials for the experiments of this study include natural transparent calcite and aragonite monocrystals which were collected from Guangxi province in southwest China, and white marble containing ~4 mol% $MgCO_3$ from Xinjiang in northwest China. The chemical compositions of the carbonate samples, which were obtained by using an ICP-OES analyzer upon dissolving 0.05 g of each sample in 10 ml hydrochloric acid (10 wt%) at 80°C, are listed in Table 1. Carbonate mineral fragments measuring 50 – 100 μm in length and width and ~30 μm in thickness were selected and loaded into the sample chamber of a Bassett type (Bassett et al., 1993) hydrothermal diamond anvil cell (HDAC, Type V), which was configured by sealing two opposed low-fluorescence diamond anvils with 800 μm diameter culets against a 400 μm-in-diameter hole in the center of a 150 μm thick rhenium gasket. In order to investigate the effect of aqueous fluid on the $CaCO_3$ phase transitions, two hydrous (deionized water and 1.0 mol/L NaCl solution) and one

anhydrous (4:1 methanol-ethanol mixture) fluids were used as the pressure transmitting media in our study. Temperature of the samples was measured by using two *K*-type thermocouples attached to each of the diamond anvils, to accuracies of ±1 and ±2°C from the set point at temperatures below and above 300°C, respectively (Yuan et al., 2016). In order to avoid potential reactions between $CaCO_3$ and traditional Raman pressure sensors (e.g., quartz, zircon) under high temperature conditions, pressure inside the sample chamber was calculated by using the EOS of water (including liquid-vapor equilibrium pressure for a two-phase fluid and isochoric pressure for a one-phase fluid) under low pressure (e.g., < 0.2 GPa) conditions (Presser et al., 2008), and from the Raman peak position shift of the symmetric stretching vibration (v_1) of aragonite (Facq et al., 2014), or the spacing between the transitional (*T* mode) and librational (*L* mode) lattice vibrations ($\Delta = v_L - v_T$) of dolomite under high pressure (e.g., > 0.2 GPa) conditions (Yuan et al., 2020). Based on the attainable accuracy of ±0.1 cm^{-1} in the measured Raman peak positions, the uncertainty in pressure calibration was estimated to be ±0.1 GPa.

The Raman spectra of all carbonate samples were measured using a Renishaw inVia micro-Raman spectrometer installed at Institute of Mineral Resources, Chinese Academy of Geological Sciences. The spectrometer is equipped with a 100 mW 514.5 nm Ar^+ laser, an 1800 gr/mm grating and a Leica 10× long-working distance objective (N.A. 0.25), providing a spectral pixel resolution of 1.5 cm^{-1}. Each Raman spectrum was acquired using an acquisition time of 20 seconds in the 100 – 1200 cm^{-1} spectral region, and by accumulation of 3 repeated collections. In order to achieve an accuracy of ±0.1 cm^{-1} or better in Raman peak position measurement under ambient and elevated temperatures, a combination of external source calibration and precision peak

fitting procedures were utilized. The spectral calibration was achieved by introducing an external-source emission peak occurring at 639.42 cm^{-1} in the measured Raman spectra, which was generated from a 532 nm frequency doubled Nd:YAG laser. Precision peak fitting procedures of each select Raman peak was made using a Gauss + Lorentz or Pearson type IV amplitude function, depending on the peak symmetry (Yuan and Mayanovic, 2017), through a PeakFit v4.12 software package (SYSTAT Software Inc.).

Results

Phase transition between $CaCO_3$-I and $CaCO_3$-II

Representative Raman spectra measured from the carbonate samples from ambient to high *P-T* conditions, which were used to delineate the phase transitions among the $CaCO_3$ polymorphs, are shown in Fig. 1. The phase transition between $CaCO_3$-I and II was identified from the characteristic split of the symmetric (or in-plane) bending Raman vibration of the CO_3 triangular unit (v_4) into two bands, and the emergence of new lattice vibrations occurring between 100 and 300 cm^{-1} (marked by stars in Fig. 1) (Fong and Nicol, 1971; Liu and Mernagh, 1990; Suito et al., 2001). During the phase transition from $CaCO_3$-I to II, which generally occurs at pressures above 1.5 GPa (Bridgman, 1938; Pippinger et al., 2015), no perceptible changes in the calcite sample appearance were observed at temperatures below 400°C. However, at *P-T* conditions exceeding 450°C and 1.5 GPa, the calcite samples were observed to transform from initially thick plates having quadrilateral outlines and sharp corners, into thin parallelogrammic $CaCO_3$-II plates (Fig. 2), while using deionized water as the pressure transmitting medium. Upon cooling and decompression, $CaCO_3$-II transformed back to $CaCO_3$-I at the same *P-T* points as determined upon heating, with $CaCO_3$-II crystal appearance being

This is the peer-reviewed, final accepted version for American Mineralogist, published by the Mineralogical Society of America.
The published version is subject to change. Cite as Authors (Year) Title. American Mineralogist, in press.
DOI: https://doi.org/10.2138/am-2021-7575. http://www.minsocam.org/

preserved in the *P-T* stability field of $CaCO_3$-I (pseudomorph). Our results show that the $CaCO_3$-I ↔ II phase transition is reversible and accomplished without hysteresis, as was observed from previous studies (Fong and Nicol, 1971; Liu and Mernagh, 1990).

By controlling the density of the aqueous fluid in the HDAC sample chamber at room temperature, we were able to investigate the full extent of the $CaCO_3$-I ↔ II phase transition boundary in *P-T* space upon heating the sample. As shown in Fig. 3, our results indicate that the $CaCO_3$-I ↔ II phase equilibrium boundary exhibits a negative $\partial P/\partial T$ slope at temperatures below 300°C and then a positive $\partial P/\partial T$ slope above this temperature. The *P-T* points for the phase transition between $CaCO_3$-I and II are 1.6 GPa at 25°C, 1.5 GPa at 95°C, 1.4 GPa at 210 and 345°C, and 1.5 GPa at 500°C (Fig. 3). The phase transition pressure values in the present study are consistent with the results obtained by Bridgman (1938) and Wang (1968) at low temperatures (< 200°C), and are lower than those from Kondo et al. (1972) by about 0.1 GPa in the 25 – 500°C temperature range, which is likely caused by the discrepancies in the experimental procedures used to measure the phase transition and/or in pressure calibration. The experiments were subsequently repeated by using hydrous (deionized water and 1.0 mol/L NaCl solution) and anhydrous (a 4:1 methanol-ethanol fluid) pressure transmitting media, whereupon consistent phase transition pressures were obtained for all three fluids. This suggests that the nature of the fluid has no measurable effect on the $CaCO_3$-I ↔ II phase transition pressure under ambient and elevated temperature conditions. For the marble sample containing ~ 4 mol% $MgCO_3$, the substitution of Mg for Ca results in an increase in the phase transition pressures by about 0.7 GPa within the 25 – 200°C temperature range. Investigation of the $CaCO_3$-I → II phase transition pressure for the marble sample under higher

Always consult and cite the final, published document. See http:/www.minsocam.org or GeoscienceWorld

166 temperatures was unsuccessful, as the sample commonly transformed to aragonite at *P-T* conditions
167 above 2.0 GPa and 200°C while using an aqueous pressure transmitting medium. Otherwise,
168 pressure of the samples could not be calibrated effectively as intense fluorescence was generated by
169 the 4:1 methanol-ethanol fluid at temperatures above 200°C.

170 ## Phase transitions among $CaCO_3$-II, III and IIIb

171 The phase transition from $CaCO_3$-II to III and IIIb is characterized with pronounced changes in
172 the measured Raman spectra, including splitting of the C–O vibrations (v_1 and v_4) and breaking up of
173 the lattice vibrations into weakly-separated bands (Pippinger et al., 2015; Yuan et al., 2018), as
174 marked by upward and downward arrows, respectively, in Fig. 1. In addition, visible micro-cracks
175 can be observed in the samples during the transformation from $CaCO_3$-II or IIIb to III (Yuan et al.,
176 2018). The phase transition pressures and phase relations among $CaCO_3$-II, III and IIIb at ambient
177 temperature have been determined in our previous study (Yuan et al., 2018), where $CaCO_3$-II was
178 observed to transform simultaneously to $CaCO_3$-III and IIIb at 1.97 GPa, with $CaCO_3$-IIIb acting as
179 an intermediate metastable phase that persists momentarily during the $CaCO_3$-II → III
180 transformation.

181 Our present experimental results show that the pressure values for the $CaCO_3$-II → III/IIIb phase
182 transition, as determined from the spacing between the *T* and *L* Raman vibrations ($\Delta = v_L - v_T$) of
183 dolomite, increase from 2.0 GPa at room temperature to 2.1 GPa at 50°C, 2.3 GPa at 100°C and 2.5
184 GPa at 150°C (Fig. 3). Consistent phase transition pressure values were obtained while using
185 hydrous and anhydrous fluids as the pressure transmitting media. However, in contrast to the
186 occurrence of $CaCO_3$-IIIb in the 2.0 – 3.4 GPa pressure range for more than 72 hours (Yuan et al.,

187 2018), the Raman vibrations of $CaCO_3$-IIIb can hardly be detected during the $CaCO_3$-II → III
188 transformation at temperatures beyond 75°C, which suggests that the $CaCO_3$-IIIb structural stability
189 decreased significantly with increasing temperature. The substitution of Mg for Ca in the marble
190 sample results in an increase by about 1.3 GPa in the $CaCO_3$-II → III phase transition pressure
191 values within the 25 – 150°C temperature range. We have also made attempts but failed in
192 determining the pressure values for the $CaCO_3$-II → III phase transition under higher temperatures,
193 for the same reason as indicated for investigating the $CaCO_3$-I → II phase transition pressure for the
194 marble samples at temperatures above 200°C. In agreement with the results from previous studies
195 (Liu and Mernagh, 1990; Pippinger et al., 2015), both the $CaCO_3$-III and IIIb phases were preserved
196 in metastable states upon decompression over the *P-T* stability field of $CaCO_3$-II, and then
197 re-transformed directly to $CaCO_3$-I at pressures lower than that of the $CaCO_3$-I ↔ II phase boundary.

198 ## Transformations between $CaCO_3$-I/II and aragonite

199 Two distinct transformation processes were distinguished during the phase transitions between
200 $CaCO_3$-I/II and aragonite in the present study. In the first experiment, calcite and marble samples
201 were loaded into the HDAC sample chamber together with an aragonite fragment and deionized
202 water (Fig. 4a). The system was compressed to ~1.2 GPa and heated at a slow rate of ~ 5°C/min, and
203 acicular aragonite was observed to have initially formed on the surface of all three fragments at
204 155°C and 1.8 GPa (Fig 4b). The system was subsequently cooled down to 100°C (1.6 GPa) and
205 further to 80°C (1.5 GPa), where all aragonite specimens continued growing at a reduced rate (Figs.
206 4c and 4d). In order to exclude the possibility that the observed growth of aragonite resulted from
207 recrystallization (e.g., thinning and elongation) of the initial aragonite fragment, the $CaCO_3$-I and

This is the peer-reviewed, final accepted version for American Mineralogist, published by the Mineralogical Society of America.
The published version is subject to change. Cite as Authors (Year) Title. American Mineralogist, in press.
DOI: https://doi.org/10.2138/am-2021-7575. http://www.minsocam.org/

marble fragments were retrieved and individually reloaded into the HDAC together with some aragonite microcrystals and deionized water (Fig. 4e). As marked by black arrows in Figs. 4f – 4h, the growth of acicular aragonite (including one specimen distributed at the edge of the sample chamber and without contact with the calcite sample) occurred sporadically upon compressing and heating, and simultaneously with depletion of the calcite fragment. A similar process was observed for the marble sample while loaded with the calcite sample (Figs 4a – d) and subsequently reloaded individually into the HDAC. This suggests that the incorporation of Mg does not have observable influence on the calcite → aragonite transformation. However, this transformation process cannot be observed under similar *P-T* conditions while using the anhydrous pressure transmitting medium. These clues lead us to conclude that the $CaCO_3$-I/II → aragonite phase transition occurs first by dissolution of calcite into the aqueous fluid, followed by precipitation of aragonite from the Ca^{2+} and CO_3^{2-} in the fluid, i.e., via a dissolution-precipitation process.

Additional experiments were made to test the effect of increased heating rates (10 – 30°C/min) on the transformation from $CaCO_3$-I/II to aragonite in water via the dissolution-precipitation process. The results show that the phase transition from $CaCO_3$-I/II to aragonite occurs at higher temperatures and is accomplished more quickly (within a few to tens of seconds) under high heating rate conditions. In addition, we also observed that the shape of the aragonite aggregates varied from acicular at temperatures below 100°C, through rectangular columnar at around 200°C, to granular under temperatures above 300°C (Figs. 4i – 4l). This suggests that the aragonite crystal morphology is closely related to the phase transition temperature and crystallization rate, which has the potential to be used as a rough indicator/geothermometer.

Always consult and cite the final, published document. See http:/www.minsocam.org or GeoscienceWorld

The solid recrystallization phase transition process for the $CaCO_3$-II → aragonite transformation was observed in an experiment carried out at *P-T* conditions above 500°C and 1.7 GPa (Fig. 5). A sample containing one fragment of calcite and another of dolomite were loaded with deionized water in the HDAC. The system was heated at ~90°C/min and the pressure of the sample (upon $CaCO_3$-I → II transformation) was increased steadily while the temperature was held in the 500 – 520°C range. In this process, the transformation was observed to start at one corner of the $CaCO_3$-II sample and to proceed as a moving visible curved phase boundary line across the crystal (Fig. 5c). Unlike in dissolution-precipitation, the solid recrystallization, which involves the breaking and reforming of the Ca-O bonds and rearrangement of the Ca^{2+} cations relative to the CO_3^{2-} units (McTigue and Wenk, 1985), was found to occur only within the extent of the $CaCO_3$-II fragment in the sample. Furthermore, the transformation from $CaCO_3$-II to aragonite via solid recrystallization observed in our hydrous experiments at high *P-T* conditions is consistent both in transformation rate and in how it is manifested with the same transformation observed in high *P-T* experiments made under anhydrous conditions (Antao and Hassan, 2010; Hacker et al., 1992; Sotin and Madon, 1988).

We have also made experiments on the aragonite → $CaCO_3$-I transformation under hydrous and anhydrous conditions. Here, both dissolution-precipitation and solid recrystallization processes were observed under high temperature and low pressure conditions (Fig. 6). The aragonite → $CaCO_3$-I dissolution-precipitation transformation, which began at ~ 400°C and 110 MPa by formation of several $CaCO_3$-I nucleates (Fig. 6b), followed by continuous growth of $CaCO_3$-I microcrystals at the expense of aragonite (Figs. 6c and 6d). The dissolution-precipitation transformation was observed at *P-T* conditions down to 350°C and 0.2 GPa during short time scales (several hours). As was noted

above, it has been observed previously that as the time scale increases to weeks, the aragonite → $CaCO_3$-I transformation via dissolution-precipitation can be observed at temperatures as low as 180°C (Perdikouri et al., 2011; Perdikouri et al., 2008). The aragonite → $CaCO_3$-I transformation via recrystallization was observed to start at 490°C under anhydrous conditions, which was characterized by formation of $CaCO_3$-I on the surface of and along the micro-cracks in the aragonite fragment (Fig. 6f). The formation of the micro-cracks occurs because of the release of stress due to structural volume expansion (~8%) upon transformation from aragonite to $CaCO_3$-I (Merlini et al., 2012). Thereafter, the visible aragonite → $CaCO_3$-I transition boundary was observed to migrate until the entire aragonite crystal was replaced by $CaCO_3$-I microcrystals (Figs. 6g – 6h). The phase transition rate (accomplished within ~10 minutes) for the solid recrystallization transformation was also found to be comparable to the values obtained from previous studies (Davis and Adams, 1965; Sotin and Madon, 1988).

Discussion

Mechanisms of the phase transitions among $CaCO_3$ crystal structures

All of the $CaCO_3$ crystal structures investigated in the present study ($CaCO_3$-I, II, III, IIIb and aragonite) have layered structures with alternate stacking of Ca and CO_3 layers (Merlini et al., 2012; Merrill and Bassett, 1975; Oganov et al., 2006; Ukita et al., 2016). In $CaCO_3$-I, which has the trigonal $R\bar{3}c$ structure, the CO_3 triangle units arrange along the same orientation in a single layer and opposite orientations in nearby layers. By contrast, as first detailed by Merrill and Bassett (1975), $CaCO_3$-II has the monoclinic $P2_1/c$ structure and a similar atomic arrangement yet involves slight rotations of the CO_3 units by 11°. Accordingly, the transformation between $CaCO_3$-I and II is a

second-order displacive transition that involves rotations of the CO_3 units and has no volume discontinuity. In $CaCO_3$-III, which has the triclinic $P\bar{1}$ structure, the CO_3 units are no longer coplanar with each other and the cation sites vary in size and consist of two large, two intermediate and one small sites (Merlini et al., 2012). Accordingly, the transformation from $CaCO_3$-II to III is a first-order reconstructive process that involves rotations and tilts of the CO_3 units and displacements of the Ca cations. The $CaCO_3$-IIIb has the same $P\bar{1}$ structure but is a simpler version than that of $CaCO_3$-III, with two instead of five non-equivalent Ca coordination polyhedra, and four instead of ten formula units in each primitive unit cell (Merlini et al., 2012). The $CaCO_3$-IIIb is thermodynamically metastable and has a higher energy than the $CaCO_3$-III phase. During the $CaCO_3$-II → III phase transition occurring at 1.97 GPa under ambient temperature, coexistence of $CaCO_3$-III and IIIb was observed in the same crystal fragment, which was followed by progressive replacement of $CaCO_3$-IIIb by III at higher pressure conditions (Yuan et al., 2018). Therefore, the $CaCO_3$-II → III phase transition is in fact spanned by the transformation to $CaCO_3$-IIIb in two reconstructive sub-stages, i.e., from $CaCO_3$-II to IIIb and from $CaCO_3$-IIIb to III (Yuan et al., 2018). This partitioning of overall phase transition helps to bridge the energy gap between the $CaCO_3$-II and III crystal structures and enables the phase transition to occur more readily under ambient and low temperature conditions.

Aragonite has an orthorhombic *Pnma* structure. Unlike in $CaCO_3$-II or III/IIIb, the CO_3 units in aragonite are located on two distinct planes between two nearby Ca layers, as viewed along the c axis (Oganov et al., 2006; Ukita et al., 2016). Furthermore, the O coordination surrounding each Ca ion is octahedral in $CaCO_3$-II and III/IIIb, whereas Ca is nine-fold coordinated by O in aragonite. Therefore,

292 the phase transition from $CaCO_3$-I/II/III to aragonite cannot be accomplished by simple
293 readjustments of the Ca cation positions or rotations and tilts of the CO_3 units. Instead, it requires
294 breaking and reformation of the Ca-O chemical bonds. This process can be accomplished directly
295 under high *P-T* conditions (e.g., above 450°C and 1.5 GPa), which corresponds to the solid
296 recrystallization processes as illustrated in Figures 5 and 6e – 6h. As an indication of the energy
297 required in the recrystallization process, an activation enthalpy of 141 kJ/mol was reported for the
298 marble → aragonite phase transition (Hacker et al., 1992) and a considerably smaller value of ~90
299 kJ/mol for a single calcite crystal to aragonite transformation (Brar and Schloessin, 1979; Rubie and
300 Thompson, 1985). The $CaCO_3$-I ↔ aragonite phase transition can also occur at lower temperatures
301 (e.g., 100 – 300°C), provided it occurs in an aqueous fluid environment (see the isolines of
302 minute-scale $CaCO_3$-I ↔ aragonite transformation in Fig. 3) and is heated at a low heating rate (e.g.,
303 <10°C/min). This is because the presence of the aqueous fluid enables the lowering of the activation
304 energy required for Ca-O bond breaking and, dissolution of calcite followed by precipitation of
305 aragonite (Fig. 4) or vice versa (Figs. 6a – d). Thus, the $CaCO_3$-I ↔ aragonite transition proceeding
306 via a dissolution-precipitation process can occur at significantly lower *P-T* conditions (Fig. 3) and
307 occurs at a substantially faster rate (by several orders of magnitude) than that for the solid
308 recrystallization processes (e.g., Hacker et al., 1992; Sotin and Madon, 1988).

309 **Influence of metal cations on the stabilities of $CaCO_3$ crystal structures**

310 Natural calcite occurring in sedimentary rocks (e.g., limestone) typically contains minor
311 amounts of metal (M) cations (Mg^{2+}, Mn^{2+}, Fe^{2+} etc.) other than Ca^{2+}. These metal cations have the
312 same electrovalence but generally smaller radii than those of Ca^{2+} (Balarew et al., 1985).

313 Correspondingly, the substitution for Ca^{2+} by such metal cations in calcite leads to an increase in the
314 interatomic M-O bond strength, resulting in a concomitant increase in the vibrational frequencies
315 (Perrin et al., 2016). Furthermore, stronger M-O bond strengths also result in higher phase transition
316 pressures among the $CaCO_3$ crystal structures under ambient and high temperature conditions. For
317 example, Shi et al. (2012) reported that progressive substitution of Ca by Mn in synthetic calcite
318 results in an increase in the $CaCO_3$-I → II → III transformation pressures under ambient temperature
319 by 0.19 and 0.26 GPa/mol%, respectively, over the 5 to 40 mol% $MnCO_3$ composition range. Similar
320 results were obtained in the present study: The marble sample containing 4 mol% $MgCO_3$
321 transformed to $CaCO_3$-II at 2.3 GPa and further to $CaCO_3$-III at 3.3 GPa at 25°C, which are higher
322 than the transformation pressures of the pure calcite sample by 0.7 and 1.3 GPa, respectively. The
323 effect of metal cations on the phase transition pressures among $CaCO_3$ polymorphs ($CaCO_3$-I, II and
324 III) at elevated temperatures is comparable to the results at room temperature.

325 We conjecture that the *P-T* transition points for $CaCO_3$-I/II to aragonite transformation via solid
326 recrystallization (either hydrous or anhydrous) will be increased due to M substitution for Ca for the
327 same reasons as discussed above. However, for the transformation via aqueous-fluid-assisted
328 dissolution-precipitation, our repeated experiments show that calcite and marble samples generally
329 transform to aragonite simultaneously (Fig. 4a – 4d). This is most likely because the breaking of the
330 M-O bonds in calcite is accomplished by dissolution of the solid into the aqueous fluid, which is
331 kinetically controlled not only by the M-O chemical bond strength, but also by the occurrence of
332 dislocations, steps, ledges and holes on the crystal surfaces (Morse and Arvidson, 2002). Thus, the

effect of partial substitution for Ca by other divalent metal cations on the dissolution of calcite and the subsequent precipitation of aragonite is insignificant.

Implications

A brief summary of the *P-T* phase boundaries and transformation processes among calcite, $CaCO_3$-II, III/IIIb and aragonite is shown in Table 2. It can be seen that in contrast to the known $CaCO_3$ structural chemistry under high *P-T* conditions, most of which was obtained by using anhydrous pressure transmitting media (e.g., KCl, He, Ne) and pure $CaCO_3$ phases as the starting material (Bayarjargal et al., 2018; Litasov et al., 2017; Merrill and Bassett, 1975; Zhang et al., 2018), the results from our present study reveal the influence from incorporation of small metal cations (Mg^{2+}, Mn^{2+}, Fe^{2+} etc.) in calcite on the transformation pressures among $CaCO_3$ crystal structures under ambient and elevated temperatures, and the effect of aqueous fluid and low heating rate on the dissolution-precipitation transformation between calcite and aragonite. Based on the simulation results from 56 segments of subduction zones throughout the world (Pennistondorland et al., 2015; Syracuse et al., 2010), at vertical depths of 15 and 60 km, which correspond to pressures of 0.5 and 2.0 GPa, temperatures of the subducted slabs vary from ~20 and 250°C for some of the coldest slabs (e.g., Tonga, Java, Honshu), to 250 and 600°C for the hottest slabs (e.g., central and north Cascadia), respectively (Fig. 3). Due to the low subduction rate of the oceanic slabs (generally tens of mm per year), the heating rate of the carbonate on the slabs is generally no greater than 0.05°C per year. Moreover, considerable amounts of aqueous fluids, which result in melting of the overlying mantle wedge and formation of arc volcanos in the convergent plate margins, are generated from dehydration of the subducted oceanic crust (Kessel et al., 2005; Schmidt and Poli, 1998; Ulmer and

This is the peer-reviewed, final accepted version for American Mineralogist, published by the Mineralogical Society of America.
The published version is subject to change. Cite as Authors (Year) Title. American Mineralogist, in press.
DOI: https://doi.org/10.2138/am-2021-7575. http://www.minsocam.org/

354 Trommsdorff, 1995). All of these conditions are favorable for the transformation from $CaCO_3$-I/II to
355 aragonite via the dissolution-precipitation process. Therefore, the calcite → aragonite → $CaCO_3$-VII
356 → post aragonite should be the predominant phase transition sequence during transport of $CaCO_3$
357 into the deep earth through subduction processes, and other high pressure metastable structures
358 including $CaCO_3$-II and III/IIIb (perhaps same for $CaCO_3$-VI) should not commonly occur in
359 subduction zones.

360 ## Acknowledgment

361 This work is supported by National Natural Science Foundation of China (No. 91858206 and
362 41702039). The authors are grateful to Dr. Xin Xiong from MNR key laboratory of metallogeny and
363 mineral assessment, CAGS, for her technical support during the Raman spectroscopic measurements,
364 and to the anonymous reviewers for their critical comments and constructive suggestions on our
365 manuscript.

366

Always consult and cite the final, published document. See http:/www.minsocam.org or GeoscienceWorld

This is the peer-reviewed, final accepted version for American Mineralogist, published by the Mineralogical Society of America.
The published version is subject to change. Cite as Authors (Year) Title. American Mineralogist, in press.
DOI: https://doi.org/10.2138/am-2021-7575. http://www.minsocam.org/

References

Antao, S.M., and Hassan, I. (2010) Temperature dependence of the structural parameters in the transformation of aragonite to calcite, as determined from *in-situ* synchrotron powder X-Ray-difraction data. Canadian Mineralogist, 48(5), 1225-1236.

Bagdassarov, N.S., and Slutskii, A.B. (2010) Phase transformations in calcite from electrical impedance measurements. Phase Transitions, 76(12), 1015-1028.

Balarew, C., Markov, L., and Petrov, K. (1985) On the crystal structure stability of calcite-type carbonates. Crystal Research and Technology, 20(8), 1079-1084.

Bassett, W.A., Shen, A.H., Bucknum, M., and Chou, I. (1993) A new diamond anvil cell for hydrothermal studies to 2.5 GPa and from -190 to 1200 °C. Review of Scientific Instruments, 64(8), 2340-2345.

Bayarjargal, L., Fruhner, C.J., Schrodt, N., and Winkler, B. (2018) $CaCO_3$ phase diagram studied with Raman spectroscopy at pressures up to 50 GPa and high temperatures and DFT modeling. Physics of the Earth and Planetary Interiors, 281.

Brar, N.S., and Schloessin, H.H. (1979) Effects of pressure, temperature, and grain size on the kinetics of the calcite → aragonite transformation. Canadian Journal of Earth Sciences, 16(7), 1402-1418.

Brenker, F.E., Vollmer, C., Vincze, L., Vekemans, B., Szymanski, A., Janssens, K., Szaloki, I., Nasdala, L., Joswig, W., and Kaminsky, F.V. (2007) Carbonates from the lower part of transition zone or even the lower mantle. Earth and Planetary Science Letters, 260(1), 1-9.

Bridgman, P.W. (1938) The high pressure behavior of miscellaneous minerals. American Journal of Science, 237(1), 7-18.

Carter, L.B., and Dasgupta, R. (2015) Hydrous basalt-limestone interaction at crustal conditions: Implications for generation of ultracalcic melts and outflux of CO_2 at volcanic arcs. Earth & Planetary Science Letters, 427, 202-214.

Dasgupta, R., and Hirschmann, M.M. (2010) The deep carbon cycle and melting in Earth's interior. Earth and Planetary Science Letters, 298(1), 1-13.

Davis, B.L. (1964) X-ray diffraction data on two high-pressure phases of calcium carbonate. Science, 145(3631), 489-491.

Always consult and cite the final, published document. See http:/www.minsocam.org or GeoscienceWorld

This is the peer-reviewed, final accepted version for American Mineralogist, published by the Mineralogical Society of America.
The published version is subject to change. Cite as Authors (Year) Title. American Mineralogist, in press.
DOI: https://doi.org/10.2138/am-2021-7575. http://www.minsocam.org/

Davis, B.L., and Adams, L.H. (1965) Kinetics of the calcite ⇌ aragonite transformation. Journal of Geophysical Research, 70(2), 433-441.

Facq, S., Daniel, I., Montagnac, G., Cardon, H., and Sverjensky, D.A. (2014) In situ Raman study and thermodynamic model of aqueous carbonate speciation in equilibrium with aragonite under subduction zone conditions. Geochimica et Cosmochimica Acta, 132, 375-390.

Fong, M.Y., and Nicol, M. (1971) Raman Spectrum of Calcium Carbonate at High Pressures. Journal of Chemical Physics, 54(2), 579-585.

Gao, J., Niu, J., Qin, S., and Wu, X. (2017) Ultradeep diamonds originate from deep subducted sedimentary carbonates. Science China-earth Sciences, 60(2), 207-217.

Hacker, B.R., Kirby, S.H., and Bohlen, S.R. (1992) Time and metamorphic petrology: Calcite to aragonite experiments. Science, 258(5079), 110-112.

Irving, A.J., and Wyllie, P.J. (1973) Melting relationships in CaO-CO_2 and MgO-CO_2 to 36 kilobars with comments on CO_2 in the mantle. Earth and Planetary Science Letters, 20(2), 220-225.

Johannes, W., and Puhan, D. (1971) The calcite-aragonite transition, reinvestigated. Contributions to Mineralogy and Petrology, 31(1), 28-38.

Kessel, R., Schmidt, M.W., Ulmer, P., and Pettke, T. (2005) Trace element signature of subduction-zone fluids, melts and supercritical liquids at 120–180 km depth. Nature, 437(7059), 724-727.

Kondo, S., Suito, K., and Matsushima, S. (1972) Ultrasonic observation of calcite I-II inversion to 700 °C. Journal of physics of the earth, 20(3), 245-250.

Li, X., Zhang, Z., Lin, J.F., Ni, H., and Zhu, M. (2018) New High-Pressure Phase of $CaCO_3$ at the Topmost Lower Mantle: Implication for the Deep-Mantle Carbon Transportation. Geophysical Research Letters, 45(3), 1355-1360.

Li, Y., Zou, Y., Chen, T., Wang, X., Qi, X., Chen, H., Du, J., and Li, B. (2015) *P-V-T* equation of state and high-pressure behavior of $CaCO_3$ aragonite. American Mineralogist, 100(10), 2323-2329.

Litasov, K.D., and Ohtani, E. (2009) Solidus and phase relations of carbonated peridotite in the system CaO–Al_2O_3–MgO–SiO_2–Na_2O–CO_2 to the lower mantle depths. Physics of the Earth and Planetary Interiors, 177, 46-58.

Always consult and cite the final, published document. See http:/www.minsocam.org or GeoscienceWorld

This is the peer-reviewed, final accepted version for American Mineralogist, published by the Mineralogical Society of America.
The published version is subject to change. Cite as Authors (Year) Title. American Mineralogist, in press.
DOI: https://doi.org/10.2138/am-2021-7575. http://www.minsocam.org/

Litasov, K.D., Shatskiy, A., Gavryushkin, P.N., Bekhtenova, A.E., Dorogokupets, P.I., Danilov, B.S., Higo, Y., Akilbekov, A.T., and Inerbaev, T.M. (2017) *P-V-T* equation of state of $CaCO_3$ aragonite to 29GPa and 1673K: In situ X-ray diffraction study. Physics of the Earth and Planetary Interiors, 265, 82-91.

Liu, J., Caracas, R., Fan, D., Bobocioiu, E., Zhang, D., and Mao, W.L. (2016) High-pressure compressibility and vibrational properties of $(Ca,Mn)CO_3$. American Mineralogist, 101(12), 2723-2730.

Liu, L.-G., and Mernagh, T.P. (1990) Phase transitions and Raman spectra of calcite at high pressures and room temperature. American Mineralogist, 75(7-8), 801-806.

Liu, M., and Yund, R.A. (1993) Transformation kinetics of polycrystalline aragonite to calcite: new experimental data, modelling, and implications. Contributions to Mineralogy and Petrology, 114(4), 465-478.

Martirosyan, N.S., Litasov, K.D., Lobanov, S.S., Goncharov, A.F., Shatskiy, A., Ohfuji, H., and Prakapenka, V.B. (2019) The Mg-carbonate–Fe interaction: Implication for the fate of subducted carbonates and formation of diamond in the lower mantle. Geoscience frontiers, 10(4), 1449-1458.

McTigue, J.W., and Wenk, H.R. (1985) Microstructures and orientation relationships in the dry-state aragonite-calcite and calcit-lime phase transformations. American Mineralogist, 70, 1253-1261.

Merlini, M., Hanfland, M., and Crichton, W.A. (2012) $CaCO_3$-III and $CaCO_3$-VI, high-pressure polymorphs of calcite: Possible host structures for carbon in the Earth's mantle. Earth and Planetary Science Letters, 265-271.

Merrill, L., and Bassett, W.A. (1975) The crystal structure of $CaCO_3$ (II), a high-pressure metastable phase of calcium carbonate. Acta Crystallographica Section B: Structural Crystallography and Crystal Chemistry, 31(2), 343-349.

Mirwald, P.W. (1976) A differential thermal analysis study of the high-temperature polymorphism of calcite at high pressure. Contributions to Mineralogy and Petrology, 59(1), 33-40.

Morse, J.W., and Arvidson, R.S. (2002) The dissolution kinetics of major sedimentary carbonate minerals. Earth-Science Reviews, 58(1), 51-84.

Oganov, A.R., Glass, C.W., and Ono, S. (2006) High-pressure phases of $CaCO_3$: crystal structure prediction and experiment. Earth and Planetary Science Letters, 241(1), 95-103.

Always consult and cite the final, published document. See http:/www.minsocam.org or GeoscienceWorld

This is the peer-reviewed, final accepted version for American Mineralogist, published by the Mineralogical Society of America.
The published version is subject to change. Cite as Authors (Year) Title. American Mineralogist, in press.
DOI: https://doi.org/10.2138/am-2021-7575. http://www.minsocam.org/

Ono, S., Kikegawa, T., Ohishi, Y., and Tsuchiya, J. (2005) Post-aragonite phase transformation in $CaCO_3$ at 40 GPa. American Mineralogist, 90(4), 667-671.

Pennistondorland, S.C., Kohn, M.J., and Manning, C.E. (2015) The global range of subduction zone thermal structures from exhumed blueschists and eclogites: Rocks are hotter than models. Earth and Planetary Science Letters, 428, 243-254.

Perdikouri, C., Kasioptas, A., Geisler, T., Schmidt, B., and Putnis, A. (2011) Experimental study of the aragonite to calcite transition in aqueous solution. Geochimica et Cosmochimica Acta, 75(20), 6211-6224.

Perdikouri, C., Kasioptas, A., Putnis, C.V., and Putnis, A. (2008) The effect of fluid composition on the mechanism of the aragonite to calcite transition. Mineralogical Magazine, 72(1), 111-114.

Perrin, J., Vielzeuf, D., Laporte, D., Ricolleau, A., Rossman, G.R., and Floquet, N. (2016) Raman characterization of synthetic magnesian calcites. American Mineralogist, 101(11), 2525-2538.

Pippinger, T., Miletich, R., Merlini, M., Lotti, P., Schouwink, P., Yagi, T., Crichton, W.A., and Hanfland, M. (2015) Puzzling calcite-III dimorphism: crystallography, high-pressure behavior, and pathway of single-crystal transitions. Physics and Chemistry of Minerals, 42(1), 29-43.

Presser, V., Heis, M., and Nickel, K.G. (2008) EOS calculations for hydrothermal diamond anvil cell operation. Review of Scientific Instruments, 79(8), 085104.

Redfern, S.A.T., Salje, E.K.H., and Navrotsky, A. (1989) High-temperature enthalpy at the orientational order-disorder transition in calcite: implications for the calcite/aragonite phase equilibrium. Contributions to Mineralogy and Petrology, 101(4), 479-484.

Rubie, D.C., and Thompson, A.B. (1985) Kinetics of Metamorphic Reactions at Elevated Temperatures and Pressures: An Appraisal of Available Experimental Data. In A.B. Thompson, and D.C. Rubie, Eds. Metamorphic Reactions. Kinetics, Textures, and Deformation, p. 27-79. Springer, New York.

Schmidt, M.W., and Poli, S. (1998) Experimentally based water budgets for dehydrating slabs and consequences for arc magma generation. Earth and Planetary Science Letters, 163(1), 361-379.

Seto, Y., Hamane, D., Nagai, T., and Fujino, K. (2008) Fate of carbonates within oceanic plates subducted to the lower mantle, and a possible mechanism of diamond formation. Physics and Chemistry of Minerals, 35(4), 223-229.

Always consult and cite the final, published document. See http:/www.minsocam.org or GeoscienceWorld

This is the peer-reviewed, final accepted version for American Mineralogist, published by the Mineralogical Society of America.
The published version is subject to change. Cite as Authors (Year) Title. American Mineralogist, in press.
DOI: https://doi.org/10.2138/am-2021-7575. http://www.minsocam.org/

Shi, W., Fleet, M.E., and Shieh, S.R. (2012) High-pressure phase transitions in Ca-Mn carbonates (Ca,Mn)CO_3 studied by Raman spectroscopy. American Mineralogist, 97, 999-1001.

Sotin, C., and Madon, M. (1988) Generalized nonlinear inversion of kinetics data: application to the calcite ↔ aragonite transformation. Physics of the Earth and Planetary Interiors, 52, 159-171.

Spandler, C., Martin, L.H.J., and Pettke, T. (2012) Carbonate assimilation during magma evolution at Nisyros (Greece), South Aegean Arc: Evidence from clinopyroxenite xenoliths. Lithos, 146, 18-33.

Suito, K., Namba, J., Horikawa, T., Taniguchi, Y., Sakurai, N., Kobayashi, M., Onodera, A., Shimomura, O., and Kikegawa, T. (2001) Phase relations of $CaCO_3$ at high pressure and high temperature. American Mineralogist, 86(8-9), 997-1002.

Syracuse, E.M., Van Keken, P.E., and Abers, G.A. (2010) The global range of subduction zone thermal models. Physics of the Earth and Planetary Interiors, 183(1), 73-90.

Ukita, M., Toyoura, K., Nakamura, A., and Matsunaga, K. (2016) Pressure-induced phase transition of calcite and aragonite: A first principles study. Journal of Applied Physics, 120(14), 56-671.

Ulmer, P., and Trommsdorff, V. (1995) Serpentine stability to mantle depths and subduction-related magmatism. Science, 268(5212), 858-861.

Wallmann, K., and Aloisi, G. (2012) The Global Carbon Cycle: Geological Processes. In A.H. Knoll, D.E. Canfield, and K.O. Konhauser, Eds. Fundamentals of Geobiology, p. 20-35. John Wiley & Sons, Chichester, West Sussex, PO19 8SQ, UK.

Wang, C. (1968) Ultrasonic study of phase transition in calcite to 20 kilobars and 180 °C. Journal of Geophysical Research, 73(12), 3937-3944.

Yuan, X., Gao, C., and Gao, J. (2018) An in-situ study of the phase transitions among $CaCO_3$ high pressure polymorphs. Mineralogical Magazine, 83(2), 191-197.

Yuan, X., and Mayanovic, R.A. (2017) An Empirical Study on Raman Peak Fitting and Its Application to Raman Quantitative Research. Applied Spectroscopy, 71(10), 2325-2338.

Yuan, X., Mayanovic, R.A., and Zheng, H. (2016) Determination of pressure from measured Raman frequency shifts of anhydrite and its application in fluid inclusions and HDAC experiments. Geochimica et Cosmochimica Acta, 194, 253-265.

Always consult and cite the final, published document. See http:/www.minsocam.org or GeoscienceWorld

This is the peer-reviewed, final accepted version for American Mineralogist, published by the Mineralogical Society of America.
The published version is subject to change. Cite as Authors (Year) Title. American Mineralogist, in press.
DOI: https://doi.org/10.2138/am-2021-7575. http://www.minsocam.org/

Yuan, X., Xiong, X., Zhang, G., and Mayanovic, R.A. (2020) Application of calcite, Mg-calcite and dolomite as Raman pressure sensors for high pressure, high temperature studies. Journal of Raman Spectroscopy, 51, 1248-1259.

Zhang, Z., Mao, Z., Liu, X., Zhang, Y., and Brodholt, J.P. (2018) Stability and Reactions of $CaCO_3$ Polymorphs in the Earth's Deep Mantle. Journal of Geophysical Research, 123(8), 6491-6500.

Always consult and cite the final, published document. See http:/www.minsocam.org or GeoscienceWorld

This is the peer-reviewed, final accepted version for American Mineralogist, published by the Mineralogical Society of America.
The published version is subject to change. Cite as Authors (Year) Title. American Mineralogist, in press.
DOI: https://doi.org/10.2138/am-2021-7575. http://www.minsocam.org/

Tables

Table 1 Chemical composition of the carbonate samples used in our experiment, the calcite and marble samples are the same as those used in our previous study (Yuan et al., 2020).

Sample	Chemical composition (wt%)										Calculated Formula
	CaO	MgO	FeO	MnO	SrO	BaO	Na_2O	K_2O	Al_2O_3	LOI	
Calcite	55.71	0.06	0.03	0.00	0.00	0.00	0.09	0.01	0.03	44.09	$CaCO_3$
Aragonite	55.65	0.09	0.04	0.01	0.01	0.00	0.11	0.02	0.06	43.98	$CaCO_3$
Marble	51.27	1.58	0.06	0.01	0.01	0.01	0.08	0.01	0.05	46.93	$Ca_{0.959}Mg_{0.041}CO_3$

Always consult and cite the final, published document. See http:/www.minsocam.org or GeoscienceWorld

This is the peer-reviewed, final accepted version for American Mineralogist, published by the Mineralogical Society of America.
The published version is subject to change. Cite as Authors (Year) Title. American Mineralogist, in press.
DOI: https://doi.org/10.2138/am-2021-7575. http://www.minsocam.org/

513 Table 2 Summary of the phase transitions among calcite ($CaCO_3$-I), $CaCO_3$-II, III/IIIb and aragonite

Phase transition	$CaCO_3$-I → II	$CaCO_3$-II → III		$CaCO_3$-I → Aragonite	
		$CaCO_3$-II → IIIb	$CaCO_3$-IIIb → III	Solid recrystallization	Dissolution-precipitation
P-T phase boundary	• Curve shape: Parabolic; • 1.6 GPa at 23°C, 1.4 GPa at 300°C, 1.5 GPa at 500°C.	• Curve shape: Exponential; • 2.0 GPa at 23°C, 2.5 GPa at 150°C.		• Curve shape: Exponential; • 0.4 GPa at 23°C, 1.0 GPa at 500°C[1].	
Observed process	• Recrystallization at T>450°C; • Accomplishes instantly; • Reversible upon decompression.	• No visible changes; • No observable hysteresis. • $CaCO_3$-IIIb occurs at T<75°C; • Transforms directly to $CaCO_3$-I upon decompression.	• Forming micro-cracks; • Significant hysteresis.	• Progressive replacement; • Significant hysteresis; • Observable at T >400°C.	• Forming new aragonite crystals; • Significant hysteresis; • Observable at T >100°C.
Changes in Raman spectrum	• v_4 → 2 sub-bands; • 3 new lattice vibrations.	• v_1 & v_4 → 3 sub-bands[2]; • 14 lattice vibrations[2].	• v_1 & v_4 → 5 sub-bands[2]; • 12 lattice vibrations[2].	• Different lattice vibrational modes; • Lower v_4 frequency than calcite by ~7 cm^{-1}.	
Transformation mechanism	• Displacive transformation[3]; • Rotations of CO_3 units by 11°[3]; • No volume discontinuity.	• Reconstructive transformation; • Displacements of Ca^{2+}, rotations and tilts of CO_3 units[4]; • Volume decrease by ~4%[4].		• Reconstructive transformation; • Breaking and reforming of Ca-O bonds; • Volume decrease by ~8%[4].	
Influential factors	• Phase transition pressure increases with progressive substitution for Ca^{2+} by smaller metal cations; • Occurs under hydrous and anhydrous conditions.				• Unaffected by incorporation of smaller metal cations; • Occurs only under hydrous conditions.

514 Note: [1] *P-T* phase boundary was determined by Redfern et al. (1989);

515 [2] Raman spectra were measured by Yuan et al. (2018), some bands were not distinguished in present study (Fig. 1);

516 [3] Phase transition mechanism was determined by Merrill and Bassett (1975);

517 [4] Crystal structures and volume changes were determined by Merlini et al. (2012).

This is the peer-reviewed, final accepted version for American Mineralogist, published by the Mineralogical Society of America.
The published version is subject to change. Cite as Authors (Year) Title. American Mineralogist, in press.
DOI: https://doi.org/10.2138/am-2021-7575. http://www.minsocam.org/

518 # List of figure captions

519 Figure 1 Representative Raman spectra measured from calcite (Cal), $CaCO_3$-II (C-II), $CaCO_3$-III
520 (C-III), $CaCO_3$-IIIb (C-IIIb) and aragonite (Arg) under ambient and elevated *P-T* conditions. See text
521 for a full description of the characteristic Raman vibrational modes used to identify the $CaCO_3$
522 polymorphs of this study. The v_{532} peak in the figure is the Raman line generated by the 532 nm laser,
523 which is used for spectral calibration.
524
525 Figure 2 Photomicrographs **(a)** – **(d)** showing the phase transition from $CaCO_3$-I to II while
526 progressively heating and compressing the samples from 26°C and 0.7 GPa to 500°C and 1.8 GPa.
527 Phase transition occurred at 400°C and 1.5 GPa, with transformation from initial thick quadrilateral
528 or irregular $CaCO_3$-I fragments into thin parallelogrammic $CaCO_3$-II plates occurring under the same
529 elevated *P-T* conditions. Dolomite (Dol) was loaded as the Raman pressure sensor.
530
531 Figure 3 A revised phase diagram of $CaCO_3$ at *P-T* conditions up to 600°C and 2.5 GPa. The isolines
532 of minute-scale $CaCO_3$-I/II ↔ aragonite transformation are modified from the kinetic models
533 developed by Sotin and Madon (1988) and Hacker et al. (1992), based on the observed phase
534 transition rates of this present study. *P-T* paths of the cold and hot subducted slabs are from Syracuse
535 et al. (2010)
536
537 Figure 4 Photomicrographs of the transformations from $CaCO_3$-I/II to aragonite (Arg) through a
538 dissolution-precipitation process, with aragonite microcrystals being marked by black arrows and
539 local time shown at the left bottom corner in **(a)** – **(h)**. The $CaCO_3$-II and aragonite samples in **(e)**
540 were retrieved from those in **(d)**. **(i)** – **(l)** show the $CaCO_3$-I/II → aragonite transformation under
541 high temperature conditions. See text for description of the phase transition processes.
542
543 Figure 5 Photomicrographs of the recrystallization phase transition from $CaCO_3$-II to aragonite (Arg).
544 The recrystallization is evident through the movement of a visible curved phase boundary line across

Always consult and cite the final, published document. See http:/www.minsocam.org or GeoscienceWorld

This is the peer-reviewed, final accepted version for American Mineralogist, published by the Mineralogical Society of America.
The published version is subject to change. Cite as Authors (Year) Title. American Mineralogist, in press.
DOI: https://doi.org/10.2138/am-2021-7575. http://www.minsocam.org/

545 the crystal. Recrystallization from initial $CaCO_3$-I into parallelogrammic $CaCO_3$-II plates can be
546 observed in **(b)**. Dolomite (Dol) was loaded as the Raman pressure sensor.
547
548 Figure 6 Photomicrographs of the phase transition from aragonite (Arg) to $CaCO_3$-I through: **(a)** – **(d)**
549 dissolution-precipitation under hydrous conditions, with $CaCO_3$-I nucleates being marked by black
550 arrows in **(b)**; **(e)** – **(h)** recrystallization under anhydrous conditions, pressure was estimated by
551 treating the sample chamber as an isochoric system. See text for description of the phase transition
552 processes.

Always consult and cite the final, published document. See http:/www.minsocam.org or GeoscienceWorld

Figure 1

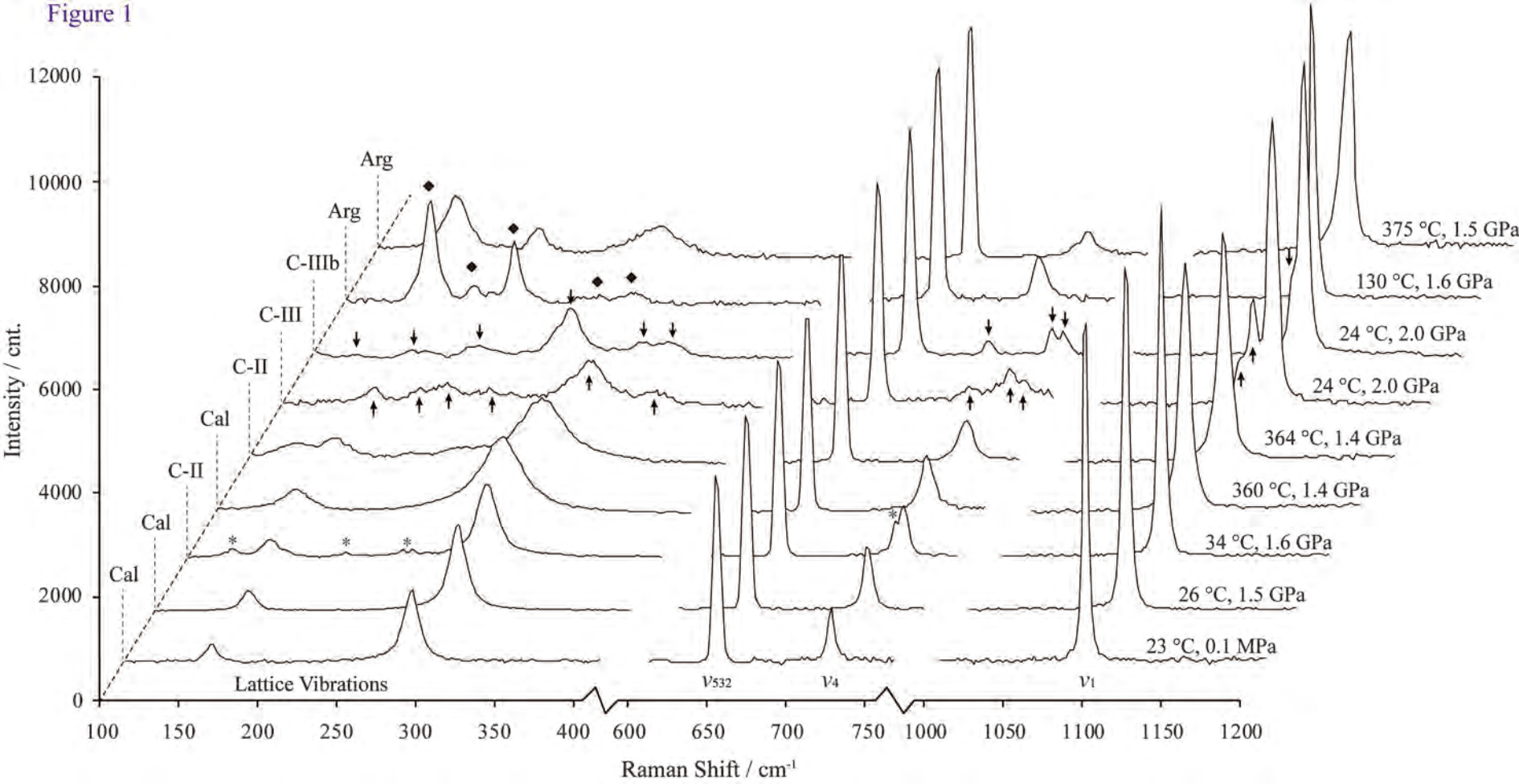
12000
10000
8000
6000
4000
2000
0
Intensity / cnt.
Arg
Arg
C-IIIb
C-III
C-II
Cal
C-II
Cal
Cal
*
*
*
*
375 °C, 1.5 GPa
130 °C, 1.6 GPa
24 °C, 2.0 GPa
24 °C, 2.0 GPa
364 °C, 1.4 GPa
360 °C, 1.4 GPa
34 °C, 1.6 GPa
26 °C, 1.5 GPa
23 °C, 0.1 MPa
Lattice Vibrations
ν532
ν4
ν1
100
150
200
250
300
350
400
600
650
700
750
1000
1050
1100
1150
1200
Raman Shift / cm-1

Figure 2

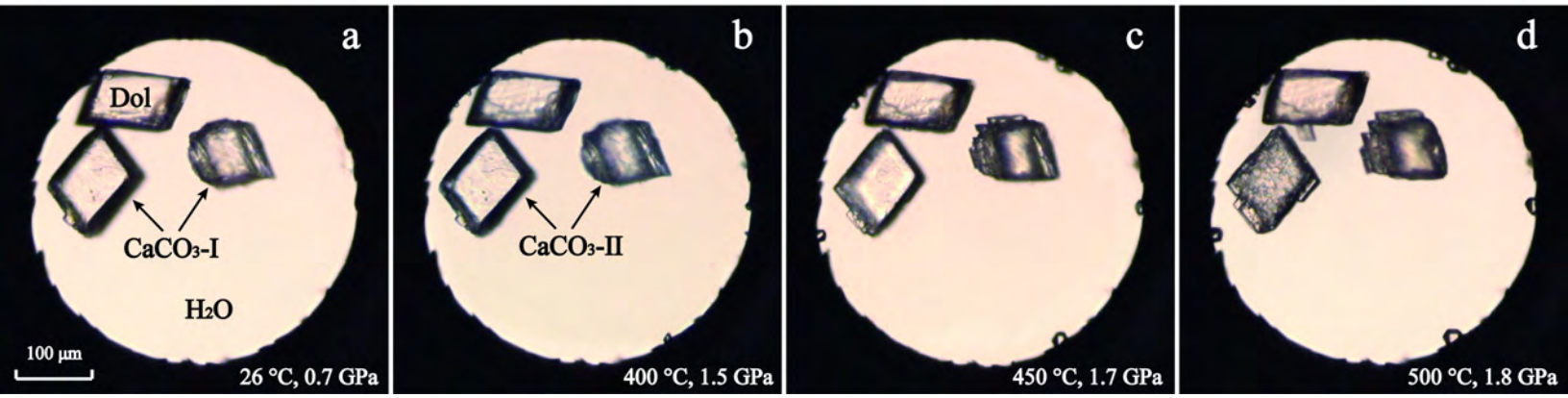
a
Dol
CaCO3-I
H2O
100 μm
26 °C, 0.7 GPa
b
CaCO3-II
400 °C, 1.5 GPa
c
450 °C, 1.7 GPa
d
500 °C, 1.8 GPa

Figure 3

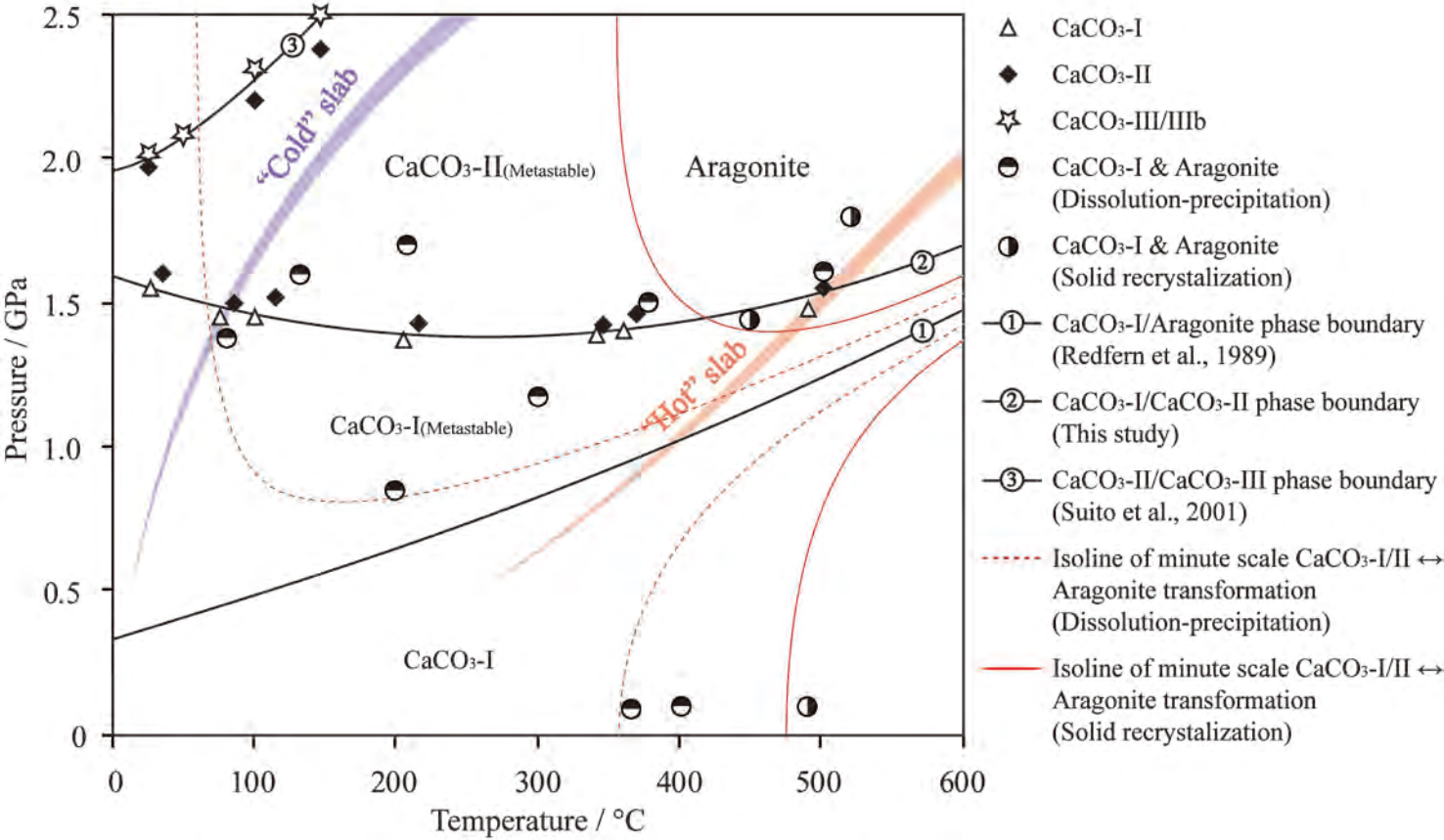
2.5
2.0
1.5
1.0
0.5
0
Pressure / GPa
0
100
200
300
400
500
600
Temperature / °C
"Cold" slab
"Hot" slab
CaCO3-II(Metastable)
Aragonite
CaCO3-I(Metastable)
CaCO3-I
CaCO3-I
CaCO3-II
CaCO3-III/IIIb
CaCO3-I & Aragonite (Dissolution-precipitation)
CaCO3-I & Aragonite (Solid recrystalization)
① CaCO3-I/Aragonite phase boundary (Redfern et al., 1989)
② CaCO3-I/CaCO3-II phase boundary (This study)
③ CaCO3-II/CaCO3-III phase boundary (Suito et al., 2001)
Isoline of minute scale CaCO3-I/II ↔ Aragonite transformation (Dissolution-precipitation)
Isoline of minute scale CaCO3-I/II ↔ Aragonite transformation (Solid recrystalization)

Figure 4

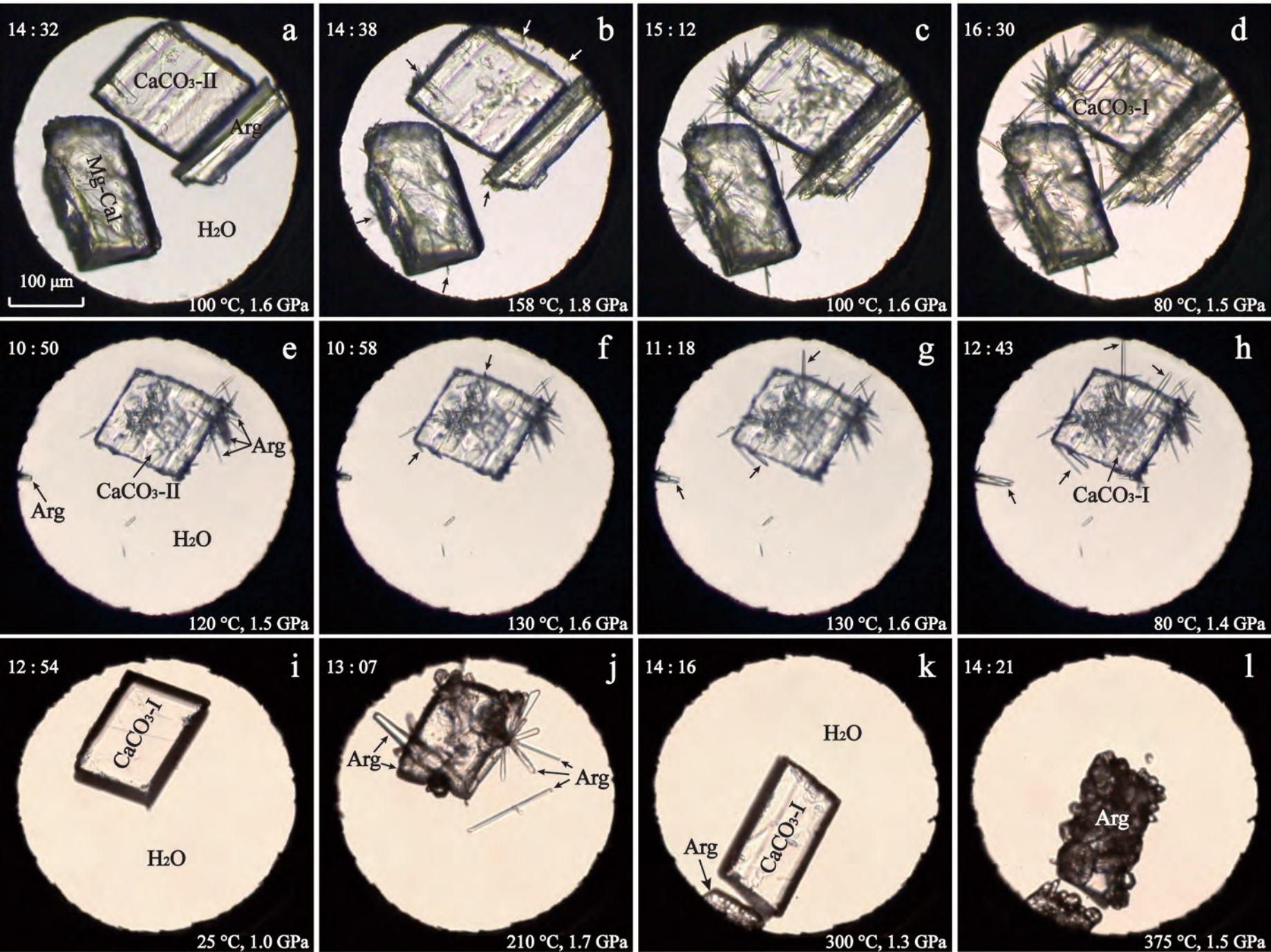
14 : 32
a
CaCO3-II
Arg
Mg-Cal
H2O
100 µm
100 °C, 1.6 GPa
14 : 38
b
158 °C, 1.8 GPa
15 : 12
c
100 °C, 1.6 GPa
16 : 30
d
CaCO3-I
80 °C, 1.5 GPa
10 : 50
e
Arg
CaCO3-II
Arg
H2O
120 °C, 1.5 GPa
10 : 58
f
130 °C, 1.6 GPa
11 : 18
g
130 °C, 1.6 GPa
12 : 43
h
CaCO3-I
80 °C, 1.4 GPa
12 : 54
i
CaCO3-I
H2O
25 °C, 1.0 GPa
13 : 07
j
Arg
Arg
210 °C, 1.7 GPa
14 : 16
k
H2O
Arg
CaCO3-I
300 °C, 1.3 GPa
14 : 21
l
Arg
375 °C, 1.5 GPa

Figure 5

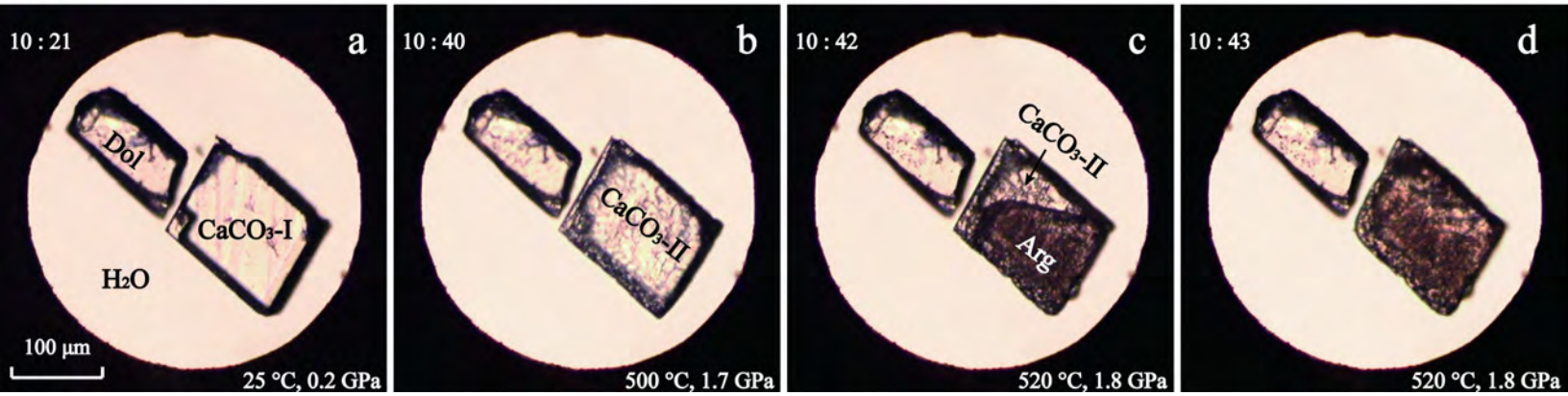
10 : 21
a
Dol
CaCO3-I
H2O
100 µm
25 °C, 0.2 GPa
10 : 40
b
CaCO3-II
500 °C, 1.7 GPa
10 : 42
c
CaCO3-II
Arg
520 °C, 1.8 GPa
10 : 43
d
520 °C, 1.8 GPa

Figure 6

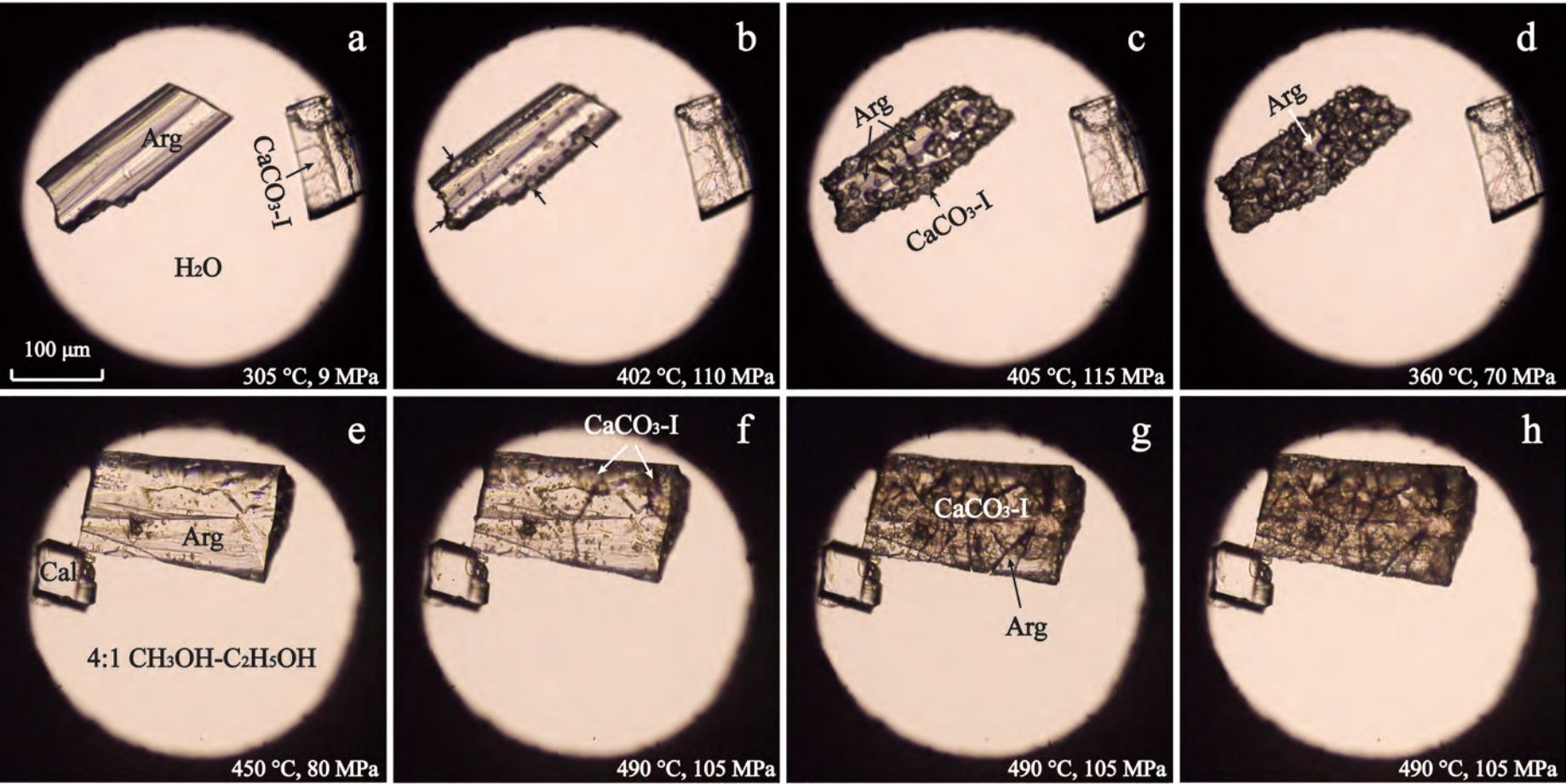
a
Arg
CaCO3-I
H2O
100 µm
305 °C, 9 MPa
b
402 °C, 110 MPa
c
Arg
CaCO3-I
405 °C, 115 MPa
d
Arg
360 °C, 70 MPa
e
Arg
Cal
4:1 CH3OH-C2H5OH
450 °C, 80 MPa
CaCO3-I
f
490 °C, 105 MPa
g
CaCO3-I
Arg
490 °C, 105 MPa
h
490 °C, 105 MPa